Cement and Concrete Research 38 (2008) 1359–1364

Contents lists available at ScienceDirect

Cement and Concrete Research

journal homepage: http://ees.elsevier.com/CEMCON/default.asp

Hydrogen bond connectivity in jennite from ab initio simulations

Sergey V. Churakov *

Paul Scherrer Institut, Laboratory for Waste Management, CH-5232 Villigen PSI, Switzerland

ARTICLE INFO

Article history:
Received 29 May 2008
Accepted 29 August 2008

Keywords:
Jennite
Ab initio simulations
Calcium–silicate–hydrate
Tobermorite

ABSTRACT

The protonation scheme and the hydrogen bond connectivity in the structure of jennite were investigated by ab initio molecular dynamics simulations. The calculated statistics of hydrogen bonds at ambient conditions is consistent with the protonation scheme proposed by Bonaccorsi et al. (2004) based on the bond valence theory. The protons in the system are associated with the ≡2Ca–OH linkage and H_2O molecules. The dangling Si–O bond on the bridging tetrahedra is de-protonated. The proton dynamics revealed in the molecular dynamic simulations explains the apparent discrepancies in the NMR and X-ray diffraction studies of jennite.

1. Introduction

Jennite and tobermorite are considered as structural prototypes for amorphous calcium–silicate–hydrates (C–S–H), which are the major components of Portland cement [1]. The jennite–tobermorite solid solution model, for example, is suggested to describe structural and thermodynamic properties of C–S–H phases with high Ca:Si ratios [2,3,1]. Hence, detailed refinements of jennite and tobermorite structures are indispensable for understanding the mechanical and chemical behaviour of cements, their sorption properties and their alternation mechanisms. The structure of tobermorite has been studied using both experimental and theoretical methods [4–9]. Recently, the structure of jennite ($Ca_9Si_6O_{18}(OH)_6{\cdot}8H_2O$) was elucidated using single crystal X-ray diffraction technique (Fig. 1). According to this model, "zeolitic" Ca5 ions hold the calcium layers of jennite via ≡2Ca–OH–Ca5–OH–2Ca≡ linkage. The Si tetrahedra form wollastonite-like chains running in the direction of the *b* axis. Protons in the structure were assigned based on the bond valence method. The detailed orientation of water molecules and OH groups, as well as the geometry of hydrogen bonds remained undefined.

In the hydrogen bonds connectivity scheme proposed by Bonaccorsi et al. [10] protons are exclusively associated with the water molecules and the ≡Ca–OH linkage [10]. ^1H–^{29}Si CP MAS NMR studies [11] suggested that some protons in the structure are associated with the ≡Si–OH linkage. Bonaccorsi et al. [10] argued that the observed NMR signal can be also explained by the presence of strong hydrogen bonds with Si–O sites. An independent approach is required to solve these apparent contradictions.

Molecular modelling is a powerful tool for accessing the structural and dynamical properties of hydrous species in mineral phases on an atomic scale. Several molecular modelling studies have been recently performed on cementitious minerals. The structure of water at the interface with tobermorite was studied by molecular dynamics (MD) using an empirical force field [12,13]. The structure of crystalline C–H–S phases was studied using ab initio, semi-empirical molecular orbital calculations and force field methods [14–18,8,19,20]. Recently, the connectivity of hydrogen bonds in the interlayer of normal and anomalous tobermorite was revealed by ab initio simulations [6,7].

The validation of the protonation scheme in jennite is the principal question addressed in this work. The ab initio quantum mechanical calculations were applied to discover the structural role of hydrous species in the interlayer of jennite starting with the structural model suggested by XRD refinement [10] and were used to interpret the previous spectroscopic studies [11,21]. The ab initio simulation technique is based on solving the electron Schrödinger equation in order to obtain the force acting on nuclei, and propagate them according to the Newton equation of motion [22]. Such calculations are computationally expensive. Nowadays, dynamic trajectories of several tens picoseconds are affordable for systems of only a few hundred atoms. A pico-second timeframe is too short to characterize slow dynamic processes such as interstitial diffusion of molecules at ambient temperature. However, it is sufficiently long to sample the basic structural parameters of crystalline phases such as bond distances. An average lifetime for hydrogen bonds is in the order of ~2 ps. So, simulations of 5–10 ps already give a valuable insight into the mechanism and extent of hydrogen bond dynamics. In this work the MD simulations of jennite were performed at 456 K and 310 K. The high temperature run was used to test the stability of the initial proton assignment. Since the probability of molecular reorientation increase

* Tel.: +41 56 310 4113; fax: +41 56 310 2821.
E-mail address: sergey.churakov@psi.ch.

0008-8846/$ – see front matter © 2008 Elsevier Ltd. All rights reserved.
doi:10.1016/j.cemconres.2008.08.004

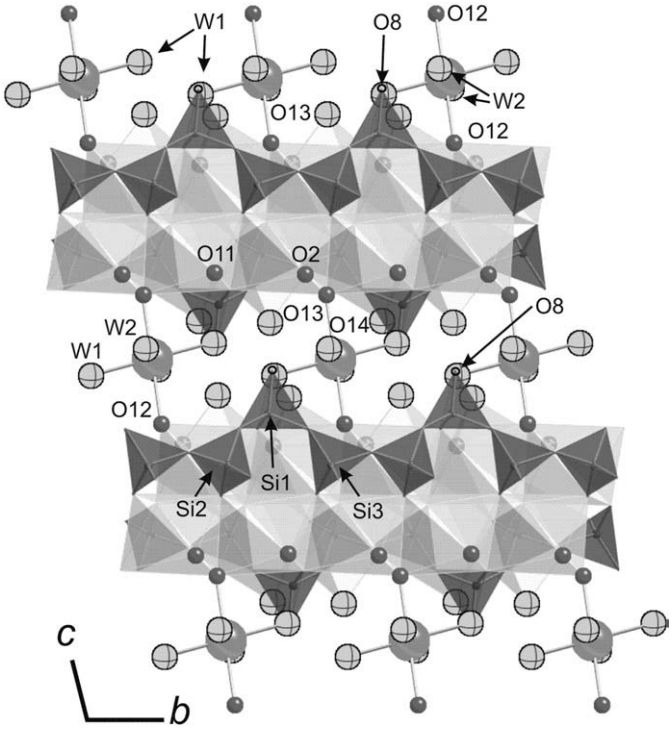

Fig. 1. Structure of jennite according to the X-ray refinements of Bonaccorsi et al. [10]. Ca and Si sites are shown as polyhedra. Interlayer Ca5 sites are shown as large gray spheres. Water molecules are represented by spheres with equatorial ellipsoids.

with the temperature the possible conformation of the molecules can be sampled more efficiently. The run at ambient temperature was used to obtain the equilibrium structure and access the proton dynamics in the jennite structure.

2. Method

The major advantage of the quantum mechanical calculations versus simulations with empirical force fields is in their ability to predict the energies and mechanisms of bond breaking/formation in arbitrary atomic configurations without prior (empirical or experimental) knowledge about the system of interest. However, such calculations are computationally expensive. Exact solution of the electron Schrödinger equation is possible only for simplest models like a hydrogen atom. For polyatomic many electron systems the quantum mechanical calculations heavily rely on various approximations (e.g. [23]). In the density functional theory [24,25] used in this work, the electrons are treated as independent particles interacting with a mean electrostatic potential produced by all electrons and nuclei cores in the system. The spatial correlation between individual electrons and the Electron Exchange (Pauli Exclusion) are taken into account in an approximate manner. A common approximation is to take the electron exchange and correlation energies to be equal to the ones of a homogeneous electron gas with the same density. In molecules and solids at ambient conditions the distribution of inner shell electrons is similar to that in an isolated atom, whereas the valence electrons continually adjust their distribution to the changing structural environment and form chemical bonds. In order to reduce computational costs the true nuclear core electrostatic potential screened by inner electrons is approximated by a pseudopotential which is obtained from isolated atom calculations. In this way only the valence electrons are treated explicitly in the calculations, while the inner shell electrons remain unchanged. Electron distribution can be represented using various mathematical expressions. Plane waves are the natural choice for crystalline solids because of their inherent periodicity. The accuracy of the plane wave representation is controlled by a plane wave cut-off. The ab initio molecular dynamics simulations rely on the Born–Oppenheimer approximation, which assumes that the electrons are remaining in their ground state during the atomic motion. Thus, at every molecular dynamic step the ground state distribution of electron in the system is calculated to obtain forces acting on the atoms.

All calculations in this work were performed using the CPMD [26] simulation package. The electron exchange and correlation were taken into account by the generalized gradient approximation BLYP [27,28]. Interaction of the valence electrons with the core states was described by the pseudopotential formalism. The core electrons were approximated by fully separable norm-conserving pseudopotentials generated using the Troullier–Martins scheme [29]. Because of significant overlap of the valence charge density with the core states of the Ca atom, the 3s and 3p electrons were treated as valence states. For the molecular dynamics simulations, the wavefunctions of valence electrons were approximated with a plane wave basis set up to 70 Ry cut-off energy. Final geometry optimization was performed using the plane wave basis set up to 120 Ry cut-off energy. The accuracy and transferability of the pseudopotentials had been tested against structures of simple oxides and hydroxides of Ca and Si as well as their molecules in gas phase. The calculated lattice parameters of the solid state oxides agree with the experimental values to within 1.5%. The bond distances were reproduced to within 1%. The identical set of pseudopotentials was used earlier in simulations of xonotlite and anomalous tobermorite [6,15].

The ab initio molecular dynamics simulations were performed in NVE ensemble using the Born–Oppenheimer approximation with a time step of 1.2 fs. Before every force evaluation step the energy was converged to 4×10^{-9} Ha/atom. The geometry of the supercell was fixed at the experimental lattice parameter values of jennite. A simulation supercell, with a composition $4\times[Ca_9Si_6O_{18}{\cdot}8H_2O]$, constructed from $2\times2\times1$ unit cells of jennite, was used throughout the simulations. A single $k=0$ point in the origin of the Brillouin zone was used in the MD simulations. The simulations were started at 456 K in order to speed up the equilibration of the system and explore the proton distribution within the limits of the short simulation time in a more efficient way. After 8 ps of the high temperature simulations, the system was annealed to the ambient conditions and equilibrated for 4 ps. Following 6 ps of the simulation trajectory at an average temperature of 310 K was used to sample the structural parameter of jennite under ambient conditions. Finally, the system was annealed to 0 K, to obtain static equilibrium geometry.

3. Results

3.1. Structural data

The atomic coordinates of jennite calculated by static geometry optimizations are compared with those obtained by the X-ray diffraction technique in Table 1. Selected inter-atomic distances averaged over MD trajectories and static geometry optimizations are summarized in Table 2. The majority of the calculated inter-atomic distances agree with the experimental ones within 2%. Exceptionally large deviations were observed for Si2–O4 and Si2–O5 contacts. The X-ray measurements give a short distance of 1.57 Å for Si2–O5 bonds and a longer one of 1.71 Å for Si2–O4. In contrast, the MD simulations suggest distances of 1.65 and 1.62 Å, for Si2–O5 and Si2–O4 contacts, respectively. It is known that the gradient corrected exchange-correlation functionals (e.g. BLYP used in this work) tend to overestimate the length of Si–O bonds [30]. This can explain the differences in the Si2–O5 distances, but contradicts the Si2–O4 contacts which are shorter in the simulations than in the XRD measurements. The simulation setup and the accuracy of the

Table 1
Fractional coordinates for jennite obtained by geometry optimization (GOpt) in the 2×2×1 supercell using 70 and 120 Ry cut-off

	GOpt 70 Ry			GOpt 120			Bonaccorsi et al. [10]		
	x	*y*	*z*	*x*	*y*	*z*	*x*	*y*	*z*
Ca1	0.060	0.359	0.364	0.061	0.360	0.364	0.0601	0.3632	0.3648
Ca2	0.418	0.797	0.362	0.418	0.798	0.364	0.4226	0.7984	0.3617
Ca3	0.066	0.862	0.379	0.066	0.862	0.379	0.0658	0.8664	0.3769
Ca4	0.428	0.292	0.350	0.426	0.291	0.350	0.4289	0.2954	0.3531
Ca5	−0.001	0.499	0.000	0.000	0.500	0.000	0.0000	0.5000	0.0000
Si1	0.801	0.939	0.188	0.802	0.939	0.188	0.8014	0.9420	0.1939
Si2	0.727	0.246	0.371	0.727	0.246	0.372	0.7248	0.2410	0.3748
Si3	0.718	0.675	0.378	0.718	0.675	0.379	0.7222	0.6730	0.3784
O1	0.964	0.013	0.243	0.965	0.014	0.244	0.9700	0.0240	0.2460
O2	0.272	0.957	0.308	0.272	0.958	0.308	0.2730	0.9620	0.3080
H2	0.228	0.917	0.217	0.229	0.917	0.218			
O3	0.588	0.130	0.418	0.588	0.130	0.418	0.5880	0.1290	0.4230
O4	0.867	0.318	0.478	0.867	0.318	0.479	0.8720	0.3180	0.4870
O5	0.745	0.122	0.235	0.746	0.123	0.236	0.7420	0.1210	0.2460
O6	0.709	0.752	0.245	0.710	0.753	0.246	0.7200	0.7470	0.2490
O7	0.702	0.438	0.324	0.702	0.438	0.326	0.7010	0.4330	0.3310
O8	0.755	0.863	0.034	0.755	0.863	0.034	0.7560	0.8590	0.0409
O9	0.579	0.660	0.433	0.579	0.661	0.433	0.5810	0.6580	0.4290
O10	0.864	0.802	0.477	0.863	0.803	0.477	0.8660	0.7940	0.4800
O11	0.274	0.450	0.303	0.274	0.452	0.303	0.2730	0.4580	0.3030
H11	0.242	0.435	0.211	0.243	0.436	0.212			
O12	0.986	0.536	0.225	0.986	0.536	0.226	0.9850	0.5420	0.2300
H12	0.886	0.482	0.214	0.887	0.482	0.215			
O13	0.452	0.166	0.128	0.451	0.168	0.128	0.4430	0.1930	0.1290
HO13′	0.372	0.155	0.055	0.373	0.156	0.056			
HO13″	0.539	0.250	0.111	0.538	0.250	0.111			
O14	0.548	0.208	0.860	0.548	0.208	0.860	0.5420	0.1910	0.8630
HO14′	0.457	0.220	0.854	0.458	0.220	0.854			
HO14″	0.537	0.069	0.871	0.537	0.071	0.870			
W1	0.909	0.138	0.935	0.909	0.139	0.934	0.9140	0.1430	0.9410
HW1′	0.959	0.073	0.879	0.959	0.075	0.879			
HW1″	0.854	0.030	0.975	0.855	0.033	0.975			
W2	0.784	0.523	0.959	0.785	0.525	0.959	0.7810	0.5190	0.9640
HW2′	0.694	0.411	0.939	0.696	0.413	0.939			
HW2″	0.769	0.657	0.991	0.770	0.657	0.991			

The X-ray diffraction data are given for comparison [10].

simulation have been carefully tested. There were no differences detected in the geometry obtained with 70 and 120 Ry cut-off (Table 1). Both MD simulations and static geometry optimization results are very close to one another. The discrepancies are most likely related to chemical and structural differences in the natural and model systems. Several studies [10,31] revealed a polytypic character of the jennite samples because of the stacking disorder and the local variation of the Ca:Si ratio which impose obvious difficulties on the accurate determination of atomic positions in the individual polytypes. In the atomistic simulations, an idealized structure with a fixed composition is considered. Local variations of the local chemistry and polytypes are not taken into account by the simulations.

3.2. Protonation scheme

A main goal of this study was to resolve discrepancies in the protonation scheme derived from X-ray diffraction [10] and NMR studies [11]. Energetically favourable distribution of the protons and the geometry of hydrogen bonds can be found either in a series of static geometry optimizations or a single MD trajectory. For a structure with a vast number of possible inter-atomic orientations, the number of configurations required to be analysed becomes prohibitively large, so that performing a single MD simulation is advantageous. Conventional MD simulations may fail to converge to the structure with the lowest energy if high energy barriers between different atomic configurations are involved. In this case, the system may remain trapped in a local energy minimum during the entire simulation time. In order to facilitate crossing such barriers, the simulations were initially performed at a temperature above the thermodynamic stability of jennite.

In the initial configuration the dangling O8 site in the bridging tetrahedra was de-protonated and was accepting hydrogen bonds from the W1, W2, and O13 water sites. During the MD simulations the protons remained preferentially attached to the W1, W2, and O13 water sites. Nevertheless, several proton transfer events along the O8…H–W2, and the O8…H–O13 contacts was observed during MD simulations at both 311 K and 456 K. The Helmholtz free energy ΔF for the proton transfer can be calculated from the proton density distribution $\rho(\Gamma)$:

$$-\frac{\Delta F(C)}{kT} = \ln[\rho(C)] + const, \quad (1)$$

where Γ is a set of internal coordinates describing the proton transfer, T is the temperature and k is the Boltzmann constant. The proton transfer along a hydrogen bond O′…H…O″ can be described as a function of the oxygen–oxygen distance R[O′…O″] and the difference between the length of R[O′…H] and R[O″…H] contacts [32]. The free energy landscape for proton transfer from W1, W2, and O13 sites to O8 site obtained at 311 K is shown in Fig. 2. Free energies for the proton transfer along the W2–H…O8 and O13–H…O8 contacts were found to be 14 ± 1.5 and 12 ± 1.5 kJ mol^{-1}, respectively. The proton transfer along the W1–H…O8 bond was not observed in the simulations at 310 K because of a higher free energy barrier (>28 kJ mol^{-1}, as estimated from the run at 456 K) and the limited simulation time. The energy barrier for the reverse transfer of a proton from the protonated O8

Table 2
Inter-atomic distances [Å] in the coordination polyhedra of the Ca and the Si sites obtained from MD simulations (maximum of the radial distribution function) and from geometry optimization (GOpt, 120 Ry cut-off) compared with the results of X-ray diffraction measurements (Exp.)

		Exp. [10]	MD 311 K	GOpt 0K
Ca1	O1	2.35	2.38 (1.2)	2.39 (1.7)
	O11	2.35	2.35 (0.1)	2.35 (0.0)
	O12	2.38	2.38 (0.1)	2.38 (0.3)
	O4[a]	2.43	2.45 (0.6)	2.47 (1.4)
	O10	2.41	2.45 (1.4)	2.48 (2.8)
Ca2	O3[a]	2.34	2.36 (0.7)	2.36 (0.9)
	O9	2.35	2.36 (0.3)	2.36 (0.5)
	O11	2.35	2.38 (1.2)	2.37 (0.8)
	O2	2.36	2.31 (2.2)	2.32 (1.7)
	O14	2.54	2.50 (1.6)	2.51 (1.2)
Ca3	O1	2.34	2.36 (1.0)	2.37 (1.3)
	O2	2.33	2.32 (0.5)	2.33 (0.2)
	O4	2.36	2.39 (1.2)	2.41 (2.0)
	O12	2.39	2.42 (1.4)	2.43 (1.7)
	O10[a]	2.46	2.44 (1.0)	2.45 (0.5)
Ca4	O2	2.34	2.33 (0.4)	2.34 (0.2)
	O9[a]	2.42	2.38 (1.8)	2.44 (0.5)
	O11	2.40	2.33 (3.0)	2.34 (2.5)
	O13	2.45	2.44 (0.6)	2.50 (1.8)
	O3	2.51	2.48 (1.2)	2.50 (0.4)
	O7	2.77	2.74 (1.1)	2.82 (1.8)
Ca5	O12	2.50	2.43 (3.0)	2.46 (2.0)
	W1	2.36	2.38 (1.0)	2.39 (1.4)
	W2	2.36	2.34 (1.0)	2.33 (1.3)
Si1	O8	1.61	1.62 (0.4)	1.62 (0.3)
	O6	1.66	1.66 (0.1)	1.67 (0.4)
	O5	1.66	1.66 (0.0)	1.65 (0.5)
	O1	1.66	1.62 (2.6)	1.62 (2.7)
Si2	O5	1.57	1.65 (4.9)	1.65 (4.8)
	O3	1.61	1.62 (0.6)	1.63 (0.9)
	O7	1.65	1.66 (0.9)	1.66 (0.7)
	O4	1.71	1.62 (5.5)	1.63 (5.2)
Si3	O6	1.61	1.65 (2.5)	1.66 (3.0)
	O10	1.62	1.62 (0.0)	1.62 (0.2)
	O9	1.63	1.62 (0.7)	1.62 (0.5)
	O7	1.65	1.66 (0.8)	1.65 (0.5)

The numbers in brackets give the deviation from the experimental data in %.
[a] Average value out of two bonds.

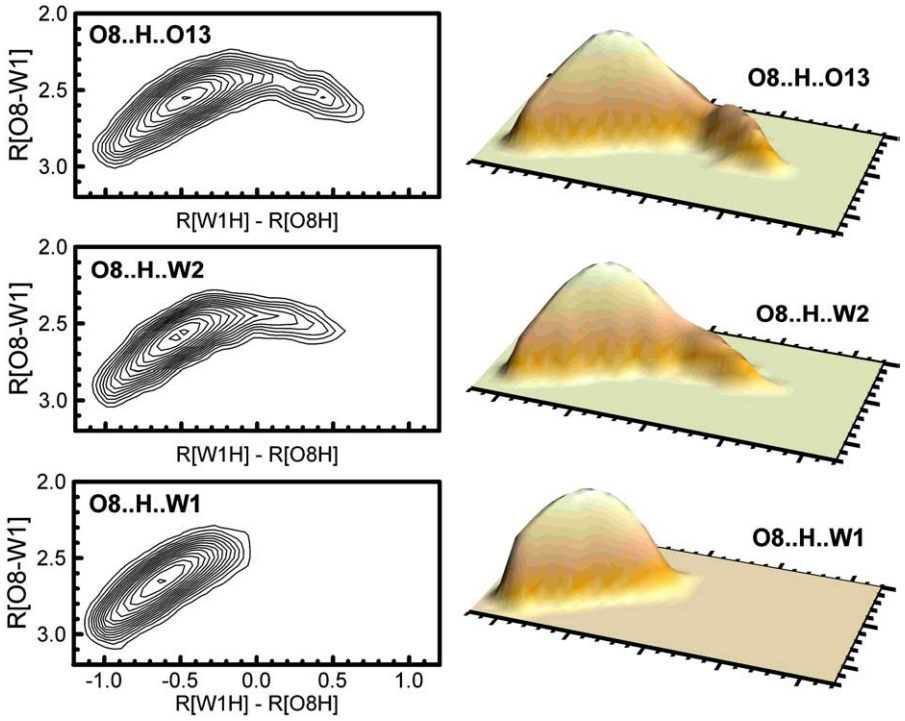

Fig. 2. Free energy $-F^*(kT)^{-1}$ landscape for proton transfer along O8…H–OX contacts (where OX is W1, W2 or O13) as a function of O8–OX distances and O8H–OXH distance differences. Contour lines are shown for every 0.5 units of reduced energy.

sites is below 1 kJ mol^{-1} indicating a very short lifetime of the O8–H…O″ configurations (where O″ is W1, W2 or O13).

The observed proton transfers to the O8 site prove the ergodicity of the simulated trajectory (e.g. the protons were not trapped in a local minimum). Although the proton may occasionally be accepted by O8 sites the protonation probability is of the order of 10^{-2}–10^{-3}. The O8 site effectively remains de-protonated, and act as a strong acceptor of hydrogen bonds. Thus, the simulations confirm the proton assignment suggested based on the bond valence theory [10].

3.3. Hydrogen bonding network

Table 3 summarizes the statistics of the hydrogen bonds in jennite. The hydrogen bonds number (n_{HB}) was defined as the value of the running coordination number at oxygen hydrogen distance of 2.4 Å. The two of the three OH groups (≡3Ca–O11H and ≡3Ca–O2H) are structurally similar to the OH groups in brucite. The third OH group (≡3Ca–O12H) forms a bridge between the Ca layer and the interlayer Ca5 sites. The interlayer Ca5 sites are six fold coordinated by four water molecule (W1, W2) and two OH groups (O12H sites). The orientation of the water molecules in the coordination shell of the Ca5 site is constrained by strong hydrogen bonds. In the W1 molecule one OH contact forms a short hydrogen bond to dangling O8 site, while the other forms a hydrogen bond with an O1 site. Similar in the W2 site, one OH contact forms a very short hydrogen bond to an O8 site, while the second one donates a hydrogen bond to the O14 water molecule. Additionally, the W1 and W2 sites accept hydrogen bonds from O2H and O12H sites respectively. The equilibrium hydrogen bonds connectivity in the interlayer of jennite is illustrated in Fig. 3.

The ≡Ca–O13H_2 and ≡Ca–O14H_2 water molecules form a row on the surface of the Ca layer running along the *b*-direction. The orientation of H′O13H″ site is constrained by a short hydrogen bond to the O8 site (O13H′…O8). The O13H″ contact is dynamically shared between the O14 and the O7 sites. In the optimized geometry the O13H″…O7 and O13H″…O14 distances are longer than 2.4 Å (Table 3). The H′O14H″ site forms one hydrogen bond to the neighbouring O13 site (O14H′…O13). The second contact O14H″ is dynamically shared among the O5, O6 and O8 sites. In the optimized geometry the O14H″…O6 contact is equal to 2.04 Å and the distances to the other sites are longer than 2.6 Å.

4. Discussion

Available NMR studies of synthetic jennite samples allow contradictory interpretations of jennite structure. Komarneni et al. [33] reported two resonance lines at −85.7 and −81.4 ppm, which were assigned to Q^2 and Q^1 sites, respectively. Further, Komarneni et al. [33] ruled out the presence of ≡Si–OH linkage in the structure. Two peaks

Table 3
Average number of hydrogen bonds n_{HB}, hydrogen bonds length [Å] at different temperatures from molecular dynamics simulations (maximum of O–H radial distribution function) and from geometry optimization (GOpt, 120 Ry cut-off)

	GOpt	MD R_{max}		n_{HB}	
	0 K	456 K	311 K	456 K	311 K
O2H…W1	1.95	1.95	1.95	0.97	0.99
O11H…W2	1.95	1.96	1.95	0.88	0.97
O12H…O5	2.61	2.63	2.60	0.14	0.14
O12H…O7	2.39	2.31	2.35	0.48	0.51
O12H…W2	2.98	2.86	2.92	0.07	0.02
O13H′…O8	1.53	1.51	1.50	1.00	1.00
O13H″…O7	2.55	2.49	2.54	0.27	0.23
O13H″…O14	2.73	–	–	0.14	0.10
O14H′…O13	1.78	1.77	1.75	0.96	1.00
O14H″…O6	2.05	2.01	2.04	0.61	0.69
O14H″…O5	2.60	2.1[a]	2.1[a]	0.36	0.30
O14H″…O8	2.64	2.3[a]	2.3[a]	0.22	0.16
W1H′…O1	1.77	1.74	1.73	1.00	1.00
W1H″…O8	1.63	1.61	1.61	1.01	1.00
W2H′…O14	1.74	1.73	1.73	1.00	1.00
W2H″…O8	1.55	1.54	1.54	1.00	1.00

– The maximum cannot be clearly identified.
[a] A shoulder without clear maxima.

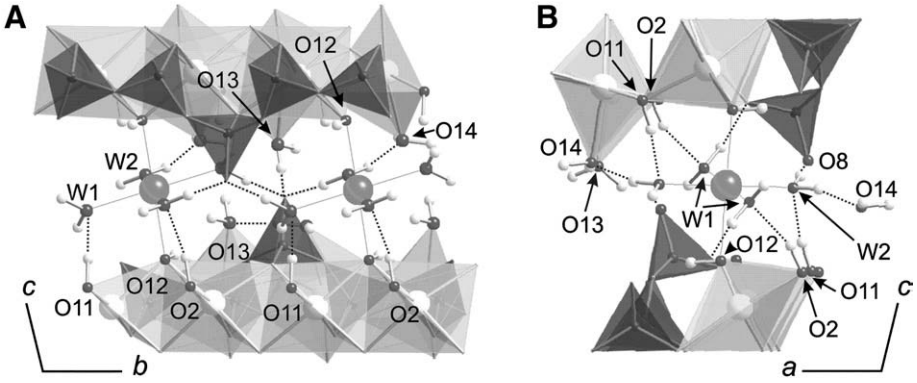

Fig. 3. Hydrogen bond (dotted lines) connectivity in the interlayer of jennite. See caption of Fig. 1 for the colour scheme. Oxygen sites of water molecules are shown as small black spheres. Hydrogen atoms are small gray spheres.

at −82.7 and −85.3 ppm observed by Cong et al. [11] were both assigned to Q^2 sites and small peaks at −80.0 ppm assigned to Q^1 sites. Based on ^1H–^{29}Si CPMAS NMR spectra it was suggested that some of the protons in the system are coupled with the tetrahedral oxygen sites [11]. The ^{17}O MAS NMR spectra were therefore fitted assuming the presence of ≡Si–OH contacts. Bonaccorsi et al. [10] pointed out that the hydrogen bond connectivity deduced from XRD results seems to contradict the structural model suggested by Cong et al. [11]. Bonaccorsi et al. further suggested that the ^1H–^{29}Si CPMAS NMR spectra can be alternatively explained by strong hydrogen bonding with the oxygen sites of silicate tetrahedra without postulating ≡Si–OH linkage. To avoid possible confusion, it should be emphasised that the ≡Si–OH linkage refers to OH groups associated with the O8 oxygen on the bridging Q^2 silica sites and not those associated with Q1 sites present in natural disordered samples due to defects in the tetrahedral chain. Such defects are not considered in the simulations.

The results of the simulated proton dynamics agree with the model derived from the X-ray diffraction studies and confirm the interpretation of ^1H–^{29}Si CP MAS NMR spectroscopy suggested by Bonaccorsi et al. [10]. The O8 site is de-protonated and accepts extremely short hydrogen bonds (1.53 to 1.63 Å) from W1, W2 and O13 H_2O sites. Vibration frequencies of the shared protons along O8…HW contacts are in 2700–3000 cm^{-1} range, as estimated from the velocity autocorrelation function at 310 K. Protons exchange with O8 sites even at room temperature, although the probability of finding a proton on an O8 site is of order 10^{-2} only. The exceptionally short O8…HW hydrogen bonds, and occasional proton transfer to O8, thus explain ^1H–^{29}Si CP MAS NMR [11]. Although the ^{17}O NMR spectra were fitted assuming the presence of ≡Si–OH groups, a fit without Si–OH should be possible, since components from ≡Si–OH and ≡Ca–OH sites overlap.

Considering, the disordered jennite structure as a prototype for amorphous C–S–H phases, it may be imagined that fragments of jennite-like tetrahedral chains occur in amorphous C–S–H phases. In particular, the presence of the bridging tetrahedra with de-protonated dangling oxygen sites (≡Si–O) can be expected. According to the simulations, such sites act as strong acceptors of hydrogen bonds and can, occasionally, become protonated. At the interface with an electrolyte solution the de-protonated tetrahedral oxygen may also act as strong sorption sites for cations in the solution. The extent of the proton exchange and sorption will depend on the pH and the composition of the equilibrium solution.

5. Conclusions

This study has identified the hydrogen bonding scheme in the idealized jennite structure. The results of the atomistic simulations confirm the proton assignment scheme proposed by Bonaccorsi et al. [10] based on XRD measurements and estimation from the bond valence theory. The O8 sites on bridging tetrahedra remain de-protonated and act as a strong acceptor of hydrogen bonds. Considering jennite as a structural prototype of the amorphous C–S–H phases, the O8 sites are the primary cation sorption sites. The present model does not include the structural heterogeneities in the interlayer of jennite. Studies of disordered structures and the influence of defects are necessary to further explore the structure of C–S–H phases.

Acknowledgments

The calculations were performed on the CRAY-XT3 cluster at the CSCS Manno. The author thanks E. Wieland and P. Mandaliev for fruitful discussion. Partial financial support was provided by the National Cooperative for the Disposal of Radioactive Waste (Nagra), Switzerland.

References

[1] I.G. Richardson, The calcium silicate hydrates, Cement and Concrete Research 38 (2008) 137–158.
[2] J.J. Chen, J.J. Thomas, H.F.W. Taylor, H.M. Jennings, Solubility and structure of calcium silicate hydrate, Cement and Concrete Research 34 (2004) 1499–1519.
[3] I.G. Richardson, Tobermorite/jennite- and tobermorite/calcium hydroxide-based models for the structure of C–S–H: applicability to hardened pastes of tricalcium silicate, beta-dicalcium silicate, Portland cement, and blends of Portland cement with blast-fumace slag, metakaolin, or silica fume, Cement and Concrete Research 34 (2004) 1733–1777.
[4] E. Bonaccorsi, S. Merlino, Crystal chemistry and structure arrangements of "normal" and "anomalous" tobermorite 11 Å, Proceedings of the sixth international congress on applied mineralogy 2 (2000) 335–338.
[5] E. Bonaccorsi, S. Merlino, A.R. Kampf, The crystal structure of tobermorite 14 Å (Plombierite), a C–S–H phase, Journal of the American Ceramic Society 88 (2005) 505–512.
[6] S.V. Churakov. Structural position of H2O molecules and hydrogen bonding in anomalous 11 Å tobermorite. American Mineralogist 94 (in press), doi:10.2138/am.2009.2907.
[7] S.V. Churakov. Structure of the interlayer in normal 11 Å tobermorite from an ab initio study. European Journal of Mineralogy (in press), doi:10.1127/0935-1221/2009/0021-1865.
[8] A. Gmira, M. Zabat, R.J.M. Pellenq, H. van Damme, Microscopic physical basis of the poromechanical behavior of cement-based materials, Materials and Structures 37 (2004) 3–14.
[9] S. Merlino, E. Bonaccorsi, T. Armbruster, The real structure of tobermorite 11 Å: normal and anomalous forms, OD character and polytypic modifications, European Journal of Mineralogy 13 (2001) 577–590.
[10] E. Bonaccorsi, S. Merlino, H. Taylor, The crystal structure of jennite, Ca9Si6O18(OH)(6)center dot 8H(2)O, Cement and Concrete Research 34 (2004) 1481–1488.
[11] X.D. Cong, R.J. Kirkpatrick, Si-29 and O-17 NMR investigation of the structure of some crystalline calcium silicate hydrates, Advanced Cement Based Materials 3 (1996) 133–143.
[12] A.G. Kalinichev, R.J. Kirkpatrick, Molecular dynamics modeling of chloride binding to the surfaces of calcium hydroxide, hydrated calcium aluminate, and calcium silicate phases, Chemistry of materials 14 (2002) 3539–3549.
[13] A.G. Kalinichev, J. Wang, R.J. Kirkpatrick, Molecular dynamics modeling of the structure, dynamics and energetics of mineral–water interfaces: application to cement materials, Cement and Concrete Research 37 (2007) 337–347.

[14] I.S. Bell, P.V. Coveney, Molecular modelling of the mechanism of action of borate retarders on hydrating cements at high temperature, Molecular Simulations 20 (1998) 331–356.
[15] S.V. Churakov, P. Mandaliev, Structure of the hydrogen bonds and silica defects in the tetrahedral double chain of xonotlite, Cement and Concrete Research 38 (2008) 300–311.
[16] P. Coveney, W. Humphries, Molecular modelling of the mechanism of action of phosphonate retarders on hydrating cements, Journal of the chemical society 92 (1996) 831–841.
[17] P. Faucon, A. Delagrave, J.C. Petit, C. Richet, J.M. Marchand, H. Zanni, Aluminum incorporation in calcium silicate hydrates (C–S–H) depending on their Ca/Si ratio, Journal of Physical Chemistry B 103 (1999) 7796–7802.
[18] P. Faucon, J.M. Delaye, J. Virlet, J.F. Jacquinot, F. Adenotg, Study of the structural properties of the C–S–H(I) by molecular dynamic simulations, Cement and Concrete Research 27 (1997) 1581–1590.
[19] S. Kashihara, S. Yamanaka, T. Inoue, T. Komatsu, H. Toyoshima, Quantum-chemical determination of the Al-substituted site in tobermorite, Journal of the American Ceramic Society 77 (1994) 3023–3026.
[20] R.J. Kirkpatrick, A.G. Kalinichev, X. Hou, L. Struble, Experimental and molecular dynamics modeling studies of interlayer swelling: water incorporation in kanemite and ASR gel, Materials and Structures 38 (2005) 449–458.
[21] P. Yu, R.J. Kirkpatrick, B. Poe, P.F. McMillan, X.D. Cong, Structure of calcium silicate hydrate (C–S–H): near-, mid-, and far-infrared spectroscopy, Journal of the American Ceramic Society 82 (1999) 742–748.
[22] M.C. Payne, M.P. Teter, D.C. Allan, T.A. Arias, J.D. Joannopoulos, Iterative minimization techniques for ab initio total-energy calculations: molecular dynamics and conjugate gradients, Review of Modern Physics 64 (1992) 1045–1097.
[23] R.M. Martin, Electronic Structure Calculations. Basic Theory and Practical Methods, Cambridge University Press, 2004.
[24] P. Hohenberg, W. Kohn, Inhomogeneous electron gas, Physical Review 136 (1964) 864–871.
[25] W. Kohn, L.J. Sham, Self-consistent equation including exchange and correlation effects, Physical Review 140 (1965) A1133–A1138.
[26] CPMD. v.3.9 Copyright IBM Corp 1990–2004, Copyright MPI fuer Festkoerperforschung Stuttgart. (1997–2001).
[27] A.D. Becke, Density-functional exchange-energy approximation with correct asymptotic behavior, Physical Review A 38 (1988) 3098–3100.
[28] C. Lee, W. Yang, R.G. Parr, Development of the Colle-Salvetti correlation-energy formula into a functional of the electron density, Physical Review B 37 (1988) 785–789.
[29] N. Troullier, J.L. Martins, Efficient pseudopotentials for plane-wave calculations, Physical Review B 43 (1991) 1993–2006.
[30] D.R. Hamman, Generalized gradient theory for silica phase transitions, Physical Review Letters 76 (1996) 660–663.
[31] D. Viehland, L.J. Yuan, Z. Xu, X.D. Cong, R.J. Kirkpatrick, Structural studies of jennite and 1.4 nm tobermorite: disordered layering along the [100] of jennite, Journal of the American Ceramic Society 80 (1997) 3021–3028.
[32] M.E. Tuckerman, D. Marx, M.L. Klein, M. Parrinello, On the quantum nature of the shated proton in hydrogen bonds, Science 275 (1997) 817–820.
[33] S. Komarneni, D.M. Roy, C.A. Fyfe, G.J. Kennedy, Naturally occurring 1.4 nm tobermorite and synthetic jennite: characterization by 27 Al and 29 Si MASNMR spectroscopy and cation exchange properties, Cement and Concrete Research 17 (1987) 891–895.